A Proposed Failure Mechanism for Pulp Fiber-Fiber Joints

Thomas Ebner,[a,e] Ulrich Hirn,[b,e,*] Wolfgang J. Fischer,[b,e] Franz J. Schmied,[c,e] Robert Schennach,[d,e] and Manfred H. Ulz [a]

Due to stress concentration at the edges, fiber-fiber bonds under load are known to fail gradually inwards from the edges. In this paper, we propose a failure mechanism for fiber-fiber joints under load, based on the peak stresses occurring at the bond edges. We have modeled the mechanical testing of individual fiber-fiber joints using a finite element method (FEM) framework. The model is based on experimental results of fiber-fiber joint strength tests designed to induce each of the three modes in fracture mechanics: opening, sliding, and tearing. A parametric study of the peak load at the edges of the fibers was carried out in order to identify a failure mechanism. The peak stresses were not directly taken from the FEM models, as these values are highly discretization-dependent. Instead, the peak stresses were estimated from resultant forces and moments in the bond and an idealized geometry of the bonding region. The literature has, up to now, focused on shear load as a failure mechanism for fiber-fiber bonds. However, our findings indicate that pulp fiber joints are sensitive to normal stresses and insensitive to shear stresses. Hence, we suggest utilizing failure criteria related to normal stress in future work.

Keywords: Failure criteria; Interfiber joint strength; Fiber-fiber bond; Shear stress; Normal stress

*Contact information: a: Institute for Strength of Materials, Graz University of Technology, 8010 Graz, Austria; b: Institute for Paper, Pulp and Fiber Technology, Graz University of Technology, 8010 Graz, Austria; c: Mondi, R&D Paper Europe & International, Theresienthalstraße 50, 3363 Ulmerfeld-Hausmening, Austria; d: Institute of Solid State Physics, Graz University of Technology, 8010 Graz, Austria; e: CD-Laboratory for Surface Chemical and Physical Fundamentals of Paper Strength, Graz University of Technology, 8010 Graz, Austria; *Corresponding author: ulrich.hirn@tugraz.at*

INTRODUCTION

The bonding strength between pulp fibers in paper is one of the key parameters determining the strength of the paper. It is not possible to measure fiber-fiber bond strength reliably from paper sheets because paper strength also depends on other factors *e.g.* fiber length, fiber tensile strength, paper density, and straining during drying of the sheet. Therefore, fiber-fiber bond strength is usually investigated by measuring the bond strength of individual fiber-fiber joints (Schniewind *et al.* 1964; Saketi and Kallio 2011; Fischer *et al.* 2012; Schmied *et al.* 2012; Saketi *et al.* 2012; Magnusson *et al.* 2013b). It might be intuitive to think that the breaking load (in N) of a fiber-fiber joint is composed of a specific bond strength (bonding force per unit area, N/m^2) times the bonded area (in m^2) of the fiber-fiber joint. This, however, is not the case. Stress concentrations occur at the edges of the bonding area (Button 1979; Uesaka 1984; Page 2002), which leads to a progressive failure of the fiber-fiber bonds starting at the peak stress regions. This progressive failure has also been observed in fiber-fiber joint testing, where sudden drops in loading force indicate local failure of the bond (Uesaka 1984; Magnusson *et al.* 2013b; Schmied *et al.* 2013).

There is considerable evidence that failure in paper also occurs due to progressive failure of fiber-fiber bonds. Nordman *et al.* (1952) found that the light scattering coefficient of paper increases upon straining. The increase in light scattering can be attributed to new surface area created in the paper due to the separation of previously bonded fiber regions (Page 2002). Investigations of fiber-fiber bonds in paper using polarized light microscopy have shown that the bonds indeed fail progressively from the edges inward under dynamic load (Page *et al.* 1962) as well as under constant load, *i.e.* creep testing (DeMaio *et al.* 2006).

It is the aim of this work to propose a key mechanism of fiber-fiber bond failure based on the peak stresses occurring at the edges of the bonds. Progressive failure is always initiated by the peak stresses in the structure. Therefore, failure theories give a criterion for yield or fracture in the material by providing a scalar representation of a multiaxial state of stress, *i.e.* the normal and shear stress are combined into a single value (Brinson and Brinson 2008; Pruitt and Chakravartula 2011). It is important to understand that, in many respects, the behavior of pulp fiber is fundamentally different from classical engineering materials. Typically, pulp fibers possess a sophisticated hierarchical micro-structure (Bodig and Benjamin 1993). Therefore, classical failure theories may not directly apply. Collagen, like pulp fibers, is a viscoelastic, fibril-based biomaterial. It has been well researched, because of its relevance regarding defects and surgery of blood vessels. Still, no conclusive failure mechanism has been worked out for this material, although several different failure mechanisms have been discussed (Wang *et al.* 1997; Gasser 2011). Recently, a comprehensive finite element method (FEM) framework to model the behavior of fiber-fiber joints during mechanical testing was presented by Magnusson *et al.* (2013). The work focused on resultant forces and moments in the bonding regions and did not consider local stress concentrations. Based on that, they discussed a failure criterion according to which the bonds are more sensitive to shear load than to normal load. For further work they recommended incorporation of local stress variations, *e.g.* by cohesive zone modeling. In a recent review (Da Silva and Campilho 2012) on cohesive zone modeling, several different failure models are discussed for fiber-based composites, the literature reviewed there also does not permit a general recommendation for the case of pulp fibers.

In this work, we will propose a key mechanism of pulp fiber-fiber bond failure based on the analysis of peak stresses inferred from FEM models of fiber-fiber bond mechanical testing. We have conducted three different types of fiber-fiber bond strength measurements, each one designed to predominantly load the fiber-fiber joint in one of the three fracture modes, see Fig. 1. The parameters for the FEM models are taken from previous experiments and literature (Magnusson *et al.* 2013b). Several parameters that represent the characteristic features of the pair of bonded fibers are defined. These are fiber thickness t, fiber width w, fiber fibril angle ψ, and crossing angle Φ of the fiber-fiber joint. These parameters are varied in physically meaningful ranges in a parametric study for three different types of loading, which correspond to mode 1, mode 2, and mode 3 types of fracture. The applied loading in the numerical model was taken from the corresponding experimental results at rupture. For each parameter set and type of loading, the arising resultant shear and normal forces as well as the resultant opening, twisting, and tearing moments in the bond region were obtained with the help of a FEM model in ABAQUS (2012). These resultant forces and moments are employed to calculate estimated normal and shear stress distributions in the interfiber joint based on a simplified model of the fiber-

fiber joint geometry. Based on that, one can identify peak values for normal and shear stress for each parameter set.

The paper is organized as follows. First, the experiments on fiber-fiber joints are described, which provide the experimentally obtained parameters for the FEM model. Next, the methods section gives details about the FEM discretization and the computation of the estimated normal and shear stress distributions in the bonding region. Furthermore, the obtained peak stresses for the three types of loading are presented. The results section presents a surprising behavior: while the obtained peak values for normal stress are within the same range for the three types of loading, the peak values for shear stress are clearly in different ranges. This suggests that normal stress plays an important role in the failure of pulp fiber-fiber bonds.

EXPERIMENTAL

In fracture mechanics, there are different modes of fracture (see Fig. 1). Cracks may propagate in the plane perpendicular to normal stress (mode 1, opening), in the plane with shear stresses with the crack line perpendicular to the stresses (mode 2, sliding), or in the plane with shear stress with the crack line parallel to the shear stress (mode 3, tearing). In single fiber testing, we have performed experiments to specifically address these different fracture modes.

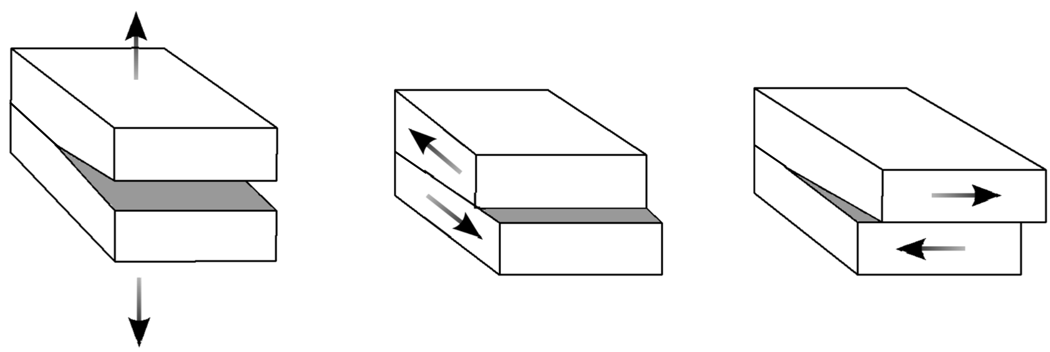

(a) Mode 1 (opening) (b) Mode 2 (sliding) (c) Mode 3 (tearing)

Fig. 1. Illustration of the three fracture modes in fracture mechanics

The experimental setup for this work is shown in Fig. 2. The details for the experimental procedure for mode 1 are described by Schmied *et al.* (2012) and for modes 2 and 3 by Fischer *et al.* (2012). In short the setups are as follows. For mode 1 an atomic force microscope (AFM) is used. The fiber-fiber bond to be tested is fixed via the top fiber (TF in Fig. 2(a)) on two sides using nail polish (NP in Fig. 2(a)). The lower fiber (LF in Fig. 2(a)) is therefore only held by the fiber bond. Then the AFM cantilever (CL in Fig. 2(a)) is used to push down the lower fiber (LF). The loading force on the lower fiber is measured with the AFM, with recording of force-distance curves. The load is applied in closest possible proximity to the fiber-fiber bonding region, thus leading to a loading situation very similar to opening mode. For mode 2 and 3 testing the fiber bonds are glued to an acrylic holder. For mode 2 the vertical fiber is glued on both sides of the holder (top part in Fig. 2(b)) and the vertical free fiber is glued to the moving part (lower part in Fig. 2(b)) to apply the force. The force distance data is obtained via a linear table, a microscope camera, and a strain gauge. For mode 3 the horizontal fiber is only fixed on one side (left side in Fig. 2(c)). Otherwise the system is identical to the mode 2 tests. The setup in Fig. 2(a) gives rise to a predominantly mode 1 load, the setup in Fig. 2(b) gives a predominantly mode 2 load, and the setup in Fig. 2(c) creates a predominantly mode 3 load. Please note that the configurations shown in Fig. 2 do not result in pure loadings according to modes 1, 2, and 3. Due to the curved geometry of the fibers, fiber twisting during the experiment, and the tilting of the fibril angle to the fiber axis, there is a large amount of opening, twisting, and tearing load on the bonding region in all three experiments (Magnusson *et al.* 2013a, b).

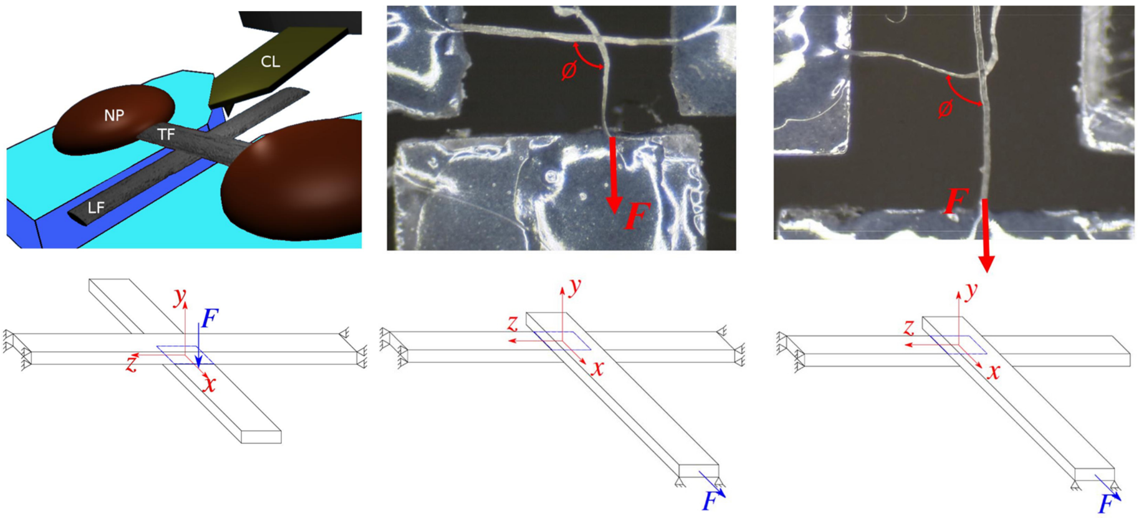

(a) Mode 1 (opening) (b) Mode 2 (sliding) c) Mode 3 (tearing)

Fig. 2. The experimental setup for the three modes

The geometry of the specimens was captured by micrographs. Furthermore, the applied force at rupture was measured. For all experiments unbleached and unrefined softwood kraft pulp fibers were used. The fiber bonds were made from highly diluted suspension put between Teflon foils in a standard lab sheet former. Therefore, all the fibers tested were collapsed. This was also checked by microscopy. For further details, we refer to (Kappel 2009).

METHODS

The objective of this work is to study the essential characteristic of fiber-fiber bonds. As mentioned in the introduction, the numerical investigation of real fibers is very challenging due to the uniqueness of each real fiber. Hence, our goal is to develop a numerical model that keeps the principal characteristics, but neglects superfluous details. The proposed numerical model is still based on experimental data, but avoids the interference with random characteristics of individual fibers. Furthermore, it allows us to make predictions on the basis of features that all fibers share.

Geometric Discretization, Material Behavior, and Loading

The cell wall of pulp fibers consists of four major layers; the primary wall and three secondary layers (S_1, S_2, S_3), as shown in Fig. 3. All layers are composed of cellulose, hemicellulose, and lignin in varying compositions (Bodig and Benjamin 1993). Furthermore, each secondary layer shows a micro-fibril wrapped helically along the fiber at a specific angle. The fiber's cell wall is made of up to 80-85% of the S_2 layer (Page 1969a), and it is commonly assumed in literature that this layer has the highest influence on the fiber's mechanical behavior (*e.g.* Magnusson and Östlund 2013). Therefore, the pulp fiber will be modeled by the S_2 layer only.

Each real pair of bonded fibers is unique. It will differ from any other pair in terms of geometry and material properties. Therefore, a system that is reduced to a minimal set of parameters is chosen to study the distinct influence of the model parameters. The fiber-fiber cross was modeled as two straight beams. Use of such a model is tantamount to neglecting the curvature and the twist along the fiber direction (Seth 2006). The model parameters were chosen to be the width w, the thickness t, and the fibril angle ψ of the fibers (Fig. 4). Furthermore, the crossing angle Φ of both fibers is investigated (Fig. 2 b,c).

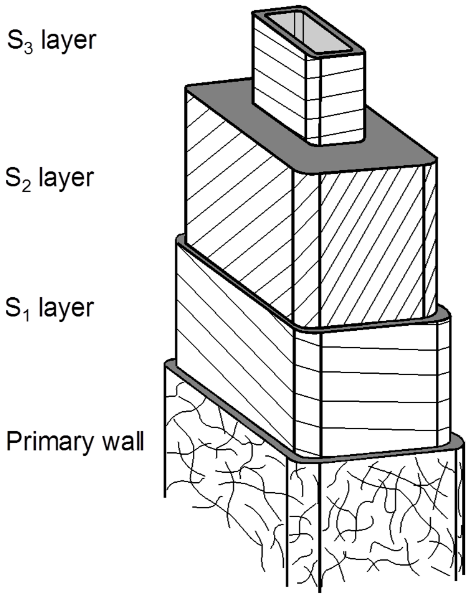

Fig. 3. The layered structure of a single pulp fiber

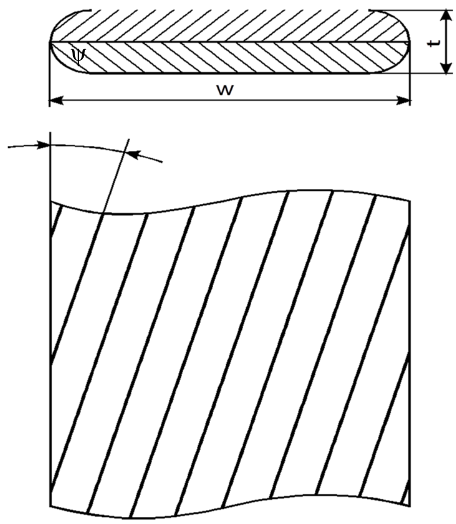

Fig. 4. Cross section and geometry of the idealized fiber structure

The fibers were considered as fully collapsed volumetric bodies. The cross section of the idealized fiber model is given in Fig. 4. Each fiber consisted of two parts with the micro-fibril pointing in opposite directions in each part. If the upper part showed an angle of $\psi = 30°$, then the lower part had -30°. The micro-fibril angle was expected to be constant along the fiber length. Furthermore, the length of the fibers was 1 mm, to be in close agreement with the previously described experiments. In all performed computations, the loaded fiber was positioned right in the middle of the fixed fiber.

The material behavior of the fiber (modeled by the S_2 layer only) was chosen to be transversely isotropic in the model. This material law considered the effect of the micro structure of the fiber. The micro-fibrils acted as a reinforcement in the matrix of lignin and hemicellulose. The axis of transverse isotropy was aligned with the direction of the micro-fibril.

The material constants as used in the simulation are shown in Table 1. The modulus of elasticity E_1=30GPa was chosen as an average of the data given by Magnusson and Östlund (2013). It has to be mentioned that the material properties of the S_2 layer are subject to wide variations (Page *et al.* 1977; Groom *et al.* 1995; Neagu *et al.* 2004). As there is not enough material data available for such a model, we are neglecting the viscoelastic nature of pulp fibers and we assume the fiber will behave according to the previously described anisotropic elastic model.

Table 1. Material Constants of the Cell Wall (Magnusson and Östlund 2013).

Coefficient	E_1	$E_2 = E_3$	$G_{12} = G_{13}$	G_{23}	$v_{12} = v_{13}$	v_{23}
Value	E_1	$\frac{E_1}{11}$	$\frac{E_1}{23}$	$\frac{E_2}{2(1+v_{23})}$	0.022	0.39

Three different modes of loading were tested according to the experiments described in the previous section. The three models of the various modes, their boundary conditions, and the direction of the applied force can be seen in Fig. 2. In modes 2 and 3, the load was applied in x-direction. If the crossing angle Φ was different to 90° and thereby the axis of the loaded fiber was not aligned to the x-direction, then the force was still applied in x-direction. In mode 1, the applied force pointed into the negative y-direction. We assumed the load to rupture the bonding region to be much smaller than the load to plastically deform or even rupture the fiber (Burgert *et al.* 2003). Hence, the bonding region was the predetermined breaking point of the structure.

Finite Element Discretization

The commercial FEM software ABAQUS (2012, version 6.11-2) and its scripting interface in Python were used to perform the non-linear quasi-static FEM model simulations. The pair of bonded fibers was discretized using a mesh consisting of 8-noded hexahedral elements with reduced integration (C3D8R in the ABAQUS element library). A mesh size dependency check was performed, and the elements' size was chosen to render the deviation in the results to be practically insignificant.

The FEM model assumed the contact area to be fully bonded, which was considered unlikely for real bonded fibers (*e.g.* Page 1960). Regions close to the edge of the bonding region, or even in the interior of the bonding region, may not be molecularly bonded (Page 1960; Kappel *et al.* 2009).

It is discussed in Torgnysdotter *et al.* (2007a, b) that the degree of contact is of great importance for the maximum stress in the bonding region. In contrast, recent results show that there is a high degree of bonding between fiber surfaces (Persson *et al.* 2013, Hirn *et al.* 2013, Hirn and Schennach 2015). Therefore, we neglected possible flaws in the bonding for reasons of simplification. Furthermore, we assumed that the contact zone did not change before rupture. As a result, the two surfaces of the fibers in contact were tied to each other by a surface-to-surface contact discretization using tie constraints in the FEM software ABAQUS. An example of the meshed pair of bonded fibers used for all three loading types is given in Fig. 5.

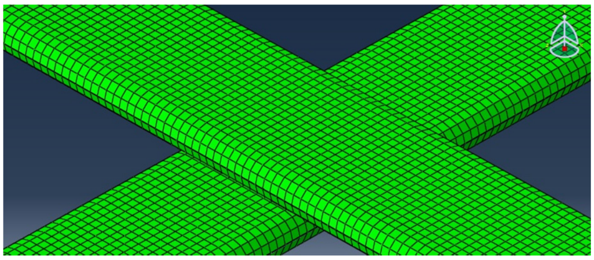

Fig. 5. Finite element model of the fiber-fiber bond.

Resultant Forces and Moments in the Bonding Region

The applied loading caused resultant reaction forces and moments in the bonding region compared with the similar treatment in Magnusson and Östlund (2013). These were described in a local coordinate system, the origin of which was defined at the centroid of the interface region. As already shown in Fig. 2, the *y*-axis was defined by the outward unit normal, *z* was defined in direction of the fixed fiber, and *x* was orthogonal to the previous two directions. The resultant reaction forces and moments in coordinate directions were computed. The resultant forces *N* (normal force), Q_x and Q_z (shear forces in x- and z-direction) were calculated by adding up the the nodal forces in the bonding region (NFORC in ABAQUS) as follows. The quantities N_i, Q_{xi}, and Q_{zi} were the nodal forces at node i (for *n* nodes in the bonding region) in *y*-, *x*-, and *z*-directions, respectively. The resultant reaction forces were computed using the three equations:

$$N = \sum_{i=1}^{n} N_i\,,\;\; Q_x = \sum_{i=1}^{n} Q_{xi}\,,\;\; Q_z = \sum_{i=1}^{n} Q_{zi} \qquad (1)$$

The three resultant moments M_x, M_y, and M_z in the local coordinate system were then obtained from the three relations:

$$M_x = \sum_{i=1}^{n} -z_i N_i\,,\;\; M_z = \sum_{i=1}^{n} x_i N_i\,,\;\; M_y = \sum_{i=1}^{n} z_i Q_{xi} - x_i Q_{zi} \qquad (2)$$

The quantities x_i and z_i were the perpendicular distances of the nodal forces to the origin of the coordinate system. Figure 6 gives a visualization of the resultant forces and moments in the bonding region.

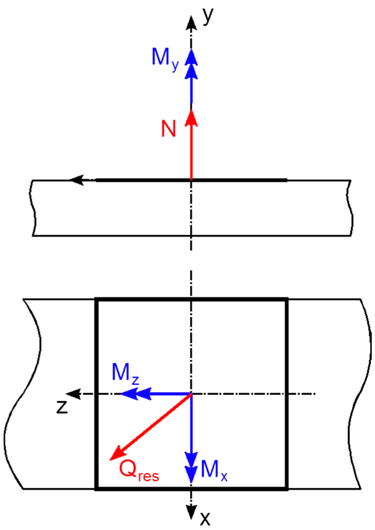

Fig. 6. Resultant forces and moments in the bonding region

Q_{res} in Fig. 6 was obtained from the equation:

$$Q_{res} = \sqrt{Q_x^2 + Q_z^2} \quad (3)$$

Resultant Stresses in the Bonding Region

Although it may appear straightforward, the peak stresses extracted directly from the FEM model of the fiber-fiber joints needed to be treated with care. For a detailed discussion on this topic, please refer to Da Silva and Campilho (2012). The peak stresses were typically found to be close to the stress discontinuities of the model, *i.e.* sharp corners or interfaces with different material properties. This was also shown by Magnusson *et al* (2013a). In the present case, this was where the rounded edge of one fiber touched the surface of the other fiber (compare Fig. 5). The magnitude of the peak stresses in the FEM model strongly depended on how well the stress field was modeled around these discontinuities. Specifically, it was very sensitive to both the mesh size used and the considered geometrical details in the model. In particular, the latter could not be appropriately met in any simplified fiber-fiber model. Therefore, we refrained from extracting the peak stresses directly from the model. Instead we applied the resulting forces and moments, as described in the previous section, to estimate the peak stresses using an idealized model of the bonding region.

The actual stress situation in fiber-fiber joints was simplified by neglecting local unbonded regions and irregularities in the fiber geometries. These simplifications were expected to lead to deviations from the reality in terms of absolute stresses. It was, however, not the present goal to correctly model the absolute values of the peak stresses or fit the experimental results to the FEM model. Instead the goal was to extract the general behavior of the peak stresses and the relation between shear- and normal stresses. This generalization was achieved, on the one hand, by simplifying the geometry of the model and, on the other hand by varying the parameters for fiber-fiber bond configurations in a wide range (see Table 2). Nevertheless, it is worth pointing out that the simplification only relates to the rectangular geometry of the bonding zone and the negligence of edge effects creating stress discontinuities, the calculation of the stresses followed standard procedures in mechanics. The presented approach computed idealized stress distributions (constant for tensile and shear loading, linear for bending and torsion) and obtained a single estimated peak value for the normal stress and a single estimated peak value for the shear stress for each pair of fibers. This allowed for an easy comparison of very different geometrical settings.

The interfacial region between the fibers in a joint was defined by the area A of the bonding region, the second area moment of inertia I for bending, and the polar section modulus W_p for torsion. As can be seen in Fig. 4, a single fiber had a radius at the edge. This had to be taken into account when the length of the bonding region was determined. Therefore, the length of the bonding region had the value w-t. For two orthogonal fibers (crossing angle Φ=90°) it was found that:

$$A = (w-t)^2,\ I = \frac{(w-t)^3(w-t)}{12},\ W_p = 0.208(w-t)^3 \quad (4)$$

The presented formula for W_p was valid only for a square section area (Grote and Feldhusen 2011). If the crossing angle Φ was different from 90°, the bonding region A changed to a rhomboid. For this case, the area A and the second area moments of inertia I_1 and I_2 were found analytically, and the torsion constant W_P was numerically computed for principal axes.

The estimated normal stress distribution σ_N, according to the resultant normal force, was constant:

$$\sigma_N = \frac{N}{A} \tag{5}$$

Next, the contribution to the normal stress due to bending σ_B for orthogonal fibers was computed as follows with M_z and M_x being the moments defined above:

$$\sigma_B = \frac{M_z}{I}x - \frac{M_x}{I}z \tag{6}$$

If the crossing angle Φ was different to 90°, σ_B was set up in principal axes. The total normal stress distribution σ_{res} was given as,

$$\sigma_{res} = \sigma_N + \sigma_B \tag{7}$$

and is visualized in Fig. 7. The maximum of the total normal stress was obtained by computing its value at the corresponding corner of the bonding region.

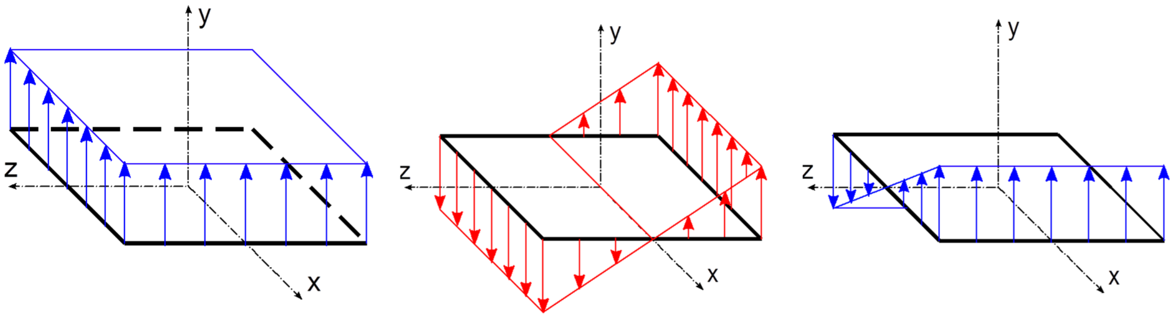

(a) normal stress (b) bending stress about the x-axis (c) bending stress about the z-axis

Fig. 7. Components of normal stress

The estimated shear stress distribution τ_{Qres} according to the resultant shear forces was assumed to be constant over the bonding region:

$$\tau_{Qres} = \frac{1}{A}\sqrt{Q_x^2 + Q_z^2} \tag{8}$$

Furthermore, the maximum shear stress due to torsion τ_T was computed as:

$$\tau_T = \frac{M_y}{W_p} \tag{9}$$

If the crossing angle Φ was different to 90°, τ_T was numerically computed. The maximum value of the total shear stress τ_{res} was found as,

$$\tau_{res} = \tau_{Qres} + \tau_T$$

and is visualized in Fig. 8.

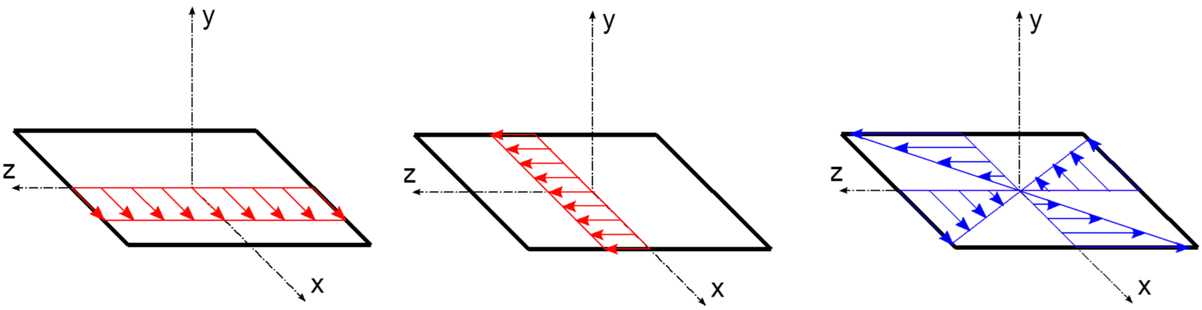

(a) shear stress in x-direction (b) shear stress in z-direction (c) torsional shear stress about the y-axis

Fig. 8. Components of shear stress.

RESULTS AND DISCUSSION

A parametric study was performed with the numerical model. The mean fiber width of the pulp was found to be 32.00 µm, and the mean fiber thickness equaled 7.45 µm. The experimentally obtained mean force in mode 1 equaled 0.33 mN (Schmied *et al.* 2013). The mean force for mode 2 was 6.45 mN, and for mode 3 it was 1.06 mN (Fischer *et al.* 2012). The ranges of the varied parameters in the numerical model are listed in Table 2 (fibril angle ψ, fiber thickness t, fiber width w, and bonding angle Φ). The applied load was taken according to the experimental results. All the conclusions drawn in the following paragraphs refer to the unbleached unrefined softwood fibers used in the experiments.

Table 2. Ranges of Modified Parameters.

	t [µm]	w [µm]	ψ [°]	Φ [°]
Range	4.65-10.25	25.20-45.60	0-45	60-120
Increments	0.70	3.40	5	5

The obtained peak values for normal and shear stresses for each parameter set and type of loading were collected and are presented in Fig. 9. The occurrence of each symbol (×, +, □) in this figure stands for a parameter set, where the shear stress in the bond is plotted against the normal stress in the bond. The three types of loading are denoted as M1, M2, and M3 (by referring to the corresponding fracture mode). The different points show the varied parameters fibril angle ψ (× in Fig. 9), fiber thickness t (+ in Fig. 9), fiber width w (◊ in Fig. 9), and bonding angle Φ (□ in Fig. 9). Furthermore, a dependency check on the applied load, Young's modulus, and Poisson's ratio (see Table 1) was performed by varying a single quantity and keeping the remaining parameters unchanged. The results were essentially equivalent to Fig. 9, and thus we refrained from reproducing them here. For each mode a "core region" of the estimated peak stresses, which contains most of the data points, can be identified in the plane of normal stress and shear stress. These core regions are marked by circles in Fig. 9.

These results showed that the obtained peak values for normal stress were within the same range between about 2 to 10 MPa for all three types of loading (all three core regions in Fig. 9 are in this range).

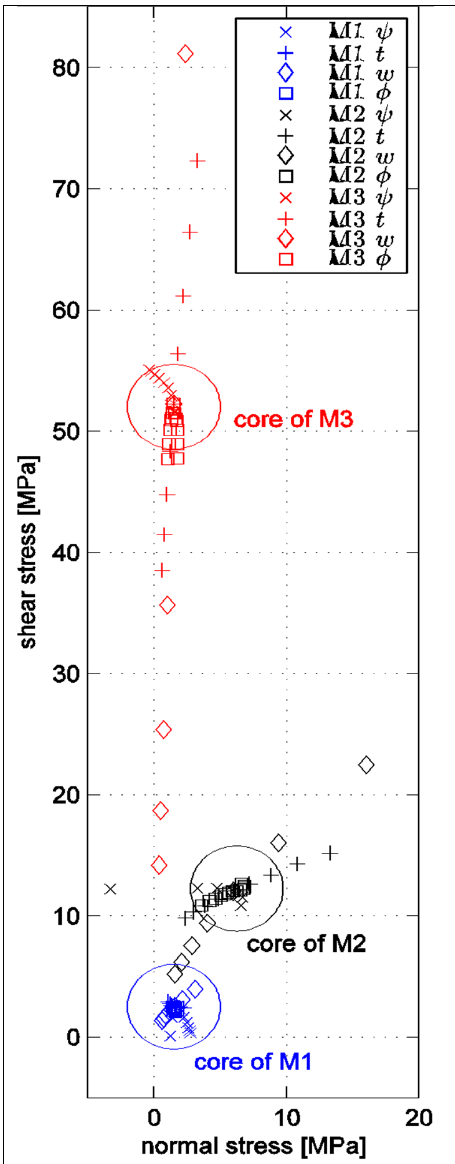

Fig. 9. Peak values of normal and shear stress of the parametric study (M1 … mode 1, M2 … mode 2, M3 … mode 3). The peak stresses form distinctive groups for the different modes of loading. While there is not very much difference in peak normal stress, the difference in peak shear stress between the groups is large: Peak shear stress is low for mode 1 load (blue), considerably higher for mode 2 load (black), and yet considerably higher for mode 3 load (red). The figure is best viewed in color.

In contrast, the core regions for shear stress were found to be in very different ranges (see Fig. 9). Mode 1 shows shear stresses around 2 to 5 MPa, Mode 2 has the core region at around 12 to 15 MPa, and Mode 3 shows values around 49 to 55 MPa. Please note that the fiber bond testing setups specifically designed to apply shear forces to the fiber-fiber bond (mode 2 and 3 in Fig. 2, M2 and M3 in Fig. 9) had the same (M3 in Fig. 9) or even higher (M2 in Fig. 9) peak normal stresses, as compared to the mode 1 (M1 in Fig. 9) configuration. The low variation in peak normal stresses and the high variation in peak shear stresses indicates that the critical factor for fiber-fiber bond strength in the experiments is the normal stress. It is not likely that the peak shear stress is the reason for failure because its core values vary from 2 to 52 MPa. It is more likely that the true limiting factor in fiber-fiber bond strength is the normal stress, which was found to have core values between 2 and 7 MPa for all experiments. The present findings thus lead to a new interpretation of the single fiber-fiber testing experiments described in the literature. The common explanation that shear stress dominates failure in fiber-fiber bonds was not found in the present results; instead the simulation results suggest that in all three types of experiments made, the bonds failed due to peak normal stresses above 2 to 7 MPa.

To place that suggestion into the right context, it is important to briefly discuss the common failure criteria applied to various materials. Material failure strongly depends on whether the material microstructure renders it ductile, brittle, or semi-brittle (Bartenev and Zuyev 1968; Collins 1981; Pruitt and Chakravartula 2011). While ductile materials yield before failure, brittle materials will instantly fracture. A semi-brittle system shows a small amount of plastic deformation prior to failure. Metals are commonly considered as ductile (Tresca or von Mises failure criteria, which are based on shear stress), and ceramics as brittle (normal stress failure criterion). The mechanical behavior of polymer structures is known to depend on many variables in a complex manner: chain chemistry, configuration and length, meso structure, and others. The failure characteristics of polymer biomaterials can exhibit both, ductile (shear stress failure) as well semi-brittle (normal stress failure) behavior (Pruitt and Chakravartula 2011). Thus our interpretation that fiber-fiber joints are more likely to be sensitive to normal loading than shear loading can be aligned with known fracture behavior of composite biomaterials from the literature.

The ideas presented in this paper have the potential to shift the understanding of how the fiber-fiber bonds in paper are failing. The fibers and the fiber-fiber bonds in paper under tensile load are subjected to shear stress because they are aligned predominantly in the paper plane. That has intuitively led to the idea that the shear stresses are responsible for the paper failure. Also, the most common theory on paper tensile strength, the equation of Page (1969b), employs shear stress as the key mechanism for fiber-fiber bond strength. As a consequence, shear load is usually regarded to be the tensile failure mechanism in paper (Page 2002). The present results, however, suggest that normal stress failure may be predominant in fiber-fiber bonds, which is a new perspective on the mechanical failure of paper under tensile load. In recent work (Magnusson and Östlund 2013; Magnusson *et al.* 2013a), it is shown that normal stresses are of considerable magnitude and present in all three different modes of loading in fiber-fiber bonds. Recently Magnusson concluded that an increase of the strength in the normal direction has the largest effect on the load carrying capacity of fiber fiber bonds (Magnusson 2016), which fits well with our finding that fiber-fiber bond failure initiates due to normal stresses.

Future work needs to expand our findings on a single fiber-fiber bond to network structures. The modes of loading and the loading history experienced by bonds in a paper network and the interaction of many pulp fibers may be different from the present model of two crossed fibers. Next to that, further experiments focusing on failure criteria of fiber-fiber joints related to normal stress are certainly required.

CONCLUSIONS

1. Fiber-fiber bonds fail gradually due to the peak stresses at the edges of the bond. A parametric study of the peak stresses in fiber-fiber joints was conducted using FEM models. The models showed characteristic core regions for the three fracture modes investigated experimentally (opening, sliding, and tearing mode). While the normal stresses are almost the same in all three cases, the shear stresses are significantly different.

2. Therefore, it was concluded that fiber-fiber joints are more likely to be sensitive to normal loading than shear loading. Hence, it is proposed that a failure criterion for fiber-fiber joints should be related to normal stress. This result brings a new perspective to the theory of fiber-fiber bond failure in paper which, in literature usually is attributed to shear failure.

REFERENCES CITED

ABAQUS FEA (2012). ABAQUS/CAE User's Manual. Dassault Systémes.

Bartenev, G. M., and Zuyev, Y. S. (1968). "Strength and failure of visco-elastic materials," Pergamon Press Ltd., Oxford.

Bodig, J., and Benjamin, A. J. (1993). "Mechanics of wood and wood composites," Krieger Publishing Company, Florida.

Brinson, H. F., and Brinson, L. C. (2008). *Polymer Engineering Science and Viscoelasticity: An Introduction*, Springer, New York.

Burgert, I., Frühmann, K., Keckes, J., Fratzl, P., and Stanzl-Tschegg, S. E. (2003). "Microtensile testing of wood fibers combined with video extensometry for efficient strain detection," *Holzforschung* 57, 661-664. DOI: 10.1515/HF.2003.099

Button, A. F. (1979). "Fiber-fiber bond strength: A study of a linear elastic model structure," Ph.D thesis, IPST, Georgia Institute of Technology.

Collins, J. A. (1981). *Failure of Materials in Mechanical Design: Analysis, Prediction, Prevention*, John Wiley & Sons, Inc., New York.

Da Silva, L. F. M., and Campilho, R. D. S. G. (2012). "Advances in numerical modeling of adhesive joints," SpringerBriefs in Applied Sciences and Technology. Springer, Berlin.

DeMaio, A., Lowe, R., Patterson, T., and Ragauskas, A. (2006). "Direct observations of bonding influence on the tensile creep behavior of paper," *Nordic Pulp & Paper Research Journal* 21, 297-302. DOI: 10.3183/NPPRJ-2006-21-03-p297-302

Fischer, W., Hirn, U., Bauer, W., and Schennach R. (2012). "Testing of individual fiber-fiber joints under biaxial load and simultaneous analysis of deformation," *Nordic Pulp & Paper Research Journal* 27, 237-244. DOI: 10.3183/NPPRJ-2012-27-02-pp. 237-244

Gasser, C. (2011). "An irreversible constitutive model for fibrous soft biological tissue: A 3-d microfiber approach with demonstrative application to abdominal aortic aneurysms," *Acta Biomaterialia* 7(6), 2457-2466. DOI: 10.1016/j.actbio.2011.02.015

Groom, L. H., Shaler, S. M., and Mott, L. (1995). "Characterizing micro and macromechanical properties of single wood fibres," in: International Paper Physics Conference, Niagara-on-the-Lake, pp. 11-14

Grote, K. H., and Feldhusen, J. (2011). "Dubbel," Springer Verlag, Berlin, 23rd edition.

Hirn, U., Schennach, R., Ganser, C., Magnusson, M., Teichert, C., and Östlund, S. (2013). "The area in molecular contact in fiber-fiber bonds," in: Trans. of the 15th Fundamental Research Symposium, Cambridge, pp. 201-226.

Hirn, U., Schennach, R. (2015). "Comprehensive analysis of individual pulp fiber bonds quantifies the mechanisms of fiber bonding in paper," *Scientific Reports* 5 10503 (9 pp.) DOI: 10.1038/srep10503

Kappel, L., Hirn, U., Bauer, W., and Schennach, R. (2009). "A novel method for the determination of bonded area of individual fiber-fiber bonds," *Nordic Pulp & Paper Research Journal* 24, 199-244. DOI: 10.3183/NPPRJ-2009-24-02-pp. 199-205

Magnusson, M. S., and Östlund, S. (2013). "Numerical evaluation of interfibre joint strength measurements in terms of three-dimensional resultant forces and moments," *Cellulose* 20, 1691-1710. DOI: 10.1007/s10570-013-9939-x

Magnusson, M. S., Fischer, J. W., Östlund, S., and Hirn, U. (2013a). "Interfibre joint strength under peeling, shearing and tearing types of loading," in: Trans. of the 15th Fundamental Research Symposium, Cambridge, pp. 103-124.

Magnusson, M. S., Zhang, X., and Östlund, S. (2013b). "Experimental evaluation of the interfibre joint strength of papermaking fibres in terms of manufacturing parameters and in two different loading directions," *Experimental Mechanics* 53, 1621-1634. DOI: 10.1007/s11340-013-9757-y

Magnusson, M. S. (2016) "Investigation of interfibre joint failure and how to tailor their properties for paper strength," *Nordic Pulp & Paper Research Journal* 31(1), 109-122. DOI: 10.3183/NPPRJ-2016-31-01-p109-122

Neagu, R. C., Gamstedt, E. K., and Lindström, M. (2004). "Influence of wood-fibre hygroexpansion on the dimensional instability of fibre mats and composites," *Composites Part A* 36, 772-788. DOI: 10.1016/j.compositesa.2004.10.023

Nordman, L., Gustafsson, C., and Gustafsson, G. (1952). "On the strength of bondings in paper," *Paperi ja Puu* 3, 47.

Page, D. H. (1960). "Fibre-to-fibre bonds part 1 - A method for their direct observation," *Paper Technology* 1, 407-411.

Page, D. H. (1969a). "A method for determining the fibrillar angle in wood tracheids," *Journal of Microscopy* 90, 137-143. DOI: 10.1111/j.1365-2818.1969.tb00701.x

Page, D. H. (1969b). "A theory for the tensile strength of paper," *Tappi Journal* 52(4), 674-681.

Page, D. H. (2002). "The meaning of Nordman bond strength," *Nordic Pulp & Paper Research Journal* 17(1), 39-44. DOI: 10.3183/NPPRJ-2002-17-01-p039-044

Page, D. H., Tydeman, P. A., and Hunt, M. (1962). "A study of fibre-to-fibre bonding by direct observation," in: Fund. Res. Symp 1961, *The Formation and Structure of Paper*, Vol. 1, pp. 171-194.

Page, D. H., El-Hosseiny, F., Winkler, F., and Lancaster, A. P. S. (1977). "Elastic modulus of single wood pulp fibres," *Tappi Journal* 60, 114-117.

Persson, B. N. J., Ganser, C., Schmied, F., Teichert, C., Schennach, R., Gilli, E., and Hirn, U. (2013). "Adhesion of cellulose fibers in paper," *J. Phys.: Condens. Matter* 25 045002 (11 pp.). DOI: 10.1088/0953-8984/25/4/045002

Pruitt, L. A., and Chakravartula, A. M. (2011). *Mechanics of Biomaterials: Fundamental Principles for Implant Design*, Cambridge University Press, Cambridge, UK.

Saketi, P., and Kallio, P. (2011). "Microrobotic platform for making, manipulating and breaking individual paper fiber bonds," in: IEEE International Symposium on Assembly and Manufacturing (ISAM), pp. 1-6.

Saketi, P., von Essen, M., Mikczinski, M., Heinemann, S., Fatikow, S., and Kallio, P. (2012). "A flexible microrobotic platform for handling microscale specimens of fibrous materials for microscopic studies," *Journal of Microscopy* 248, 163-171. DOI: 10.1111/j.1365-2818.2012.03660.x

Schmied, F., Teichert, C., Kappel, L., Hirn, U., and Schennach, R. (2012). "Joint strength measurements of individual fiber-fiber bonds an atomic force microscopy based method," *Review of Scientific Instruments* 83, 073902-1-073902-8. DOI: 10.1063/1.4731010.

Schmied, F., Teichert, C., Kappel, L., Hirn, U., Bauer, W., and Schennach, R. (2013). "What holds paper together: Nanometre scale exploration of bonding between paper fibres," *Scientific Reports* 3, 2432 1-6. DOI: 10.1038/srep02432.

Schniewind, A. P., Nemeth, L. J., and Brink, D. L. (1964). "Fiber and pulp properties - I. Shear strength of single fiber crossings," *Tappi Journal* 47, 244-248.

Seth, R. S. (2006). "The importance of fibre straightness for pulp strength," *Pulp & Paper Canada* 107, 34-42.

Torgnysdotter, A., Kulachenko, A., Gradin, P., and Wågberg, L. (2007a). "Fiber/fiber crosses: Finite element modeling and comparison with experiment," *Journal of Composite Materials* 41, 1603-1618. DOI: 10.1177/0021998306069873

Torgnysdotter, A., Kulachenko, A., Gradin, P., and Wågberg, L. (2007b). "The link between the fiber contact zone and the physical properties of paper: A way to control paper properties," *Journal of Composite Materials* 41, 1619-1633. DOI: 10.1177/0021998306069875

Uesaka, T. (1984). "Determination of fiber-fiber bond properties," in: *Handbook of Physical Testing of Paper*, CRC Press, pages 379-402.

Wang, J. L., Parnianpour, M., Shirazi-Adl, A., and Engin, A. E. (1997). "Failure criterion of collagen fiber: Viscoelastic behavior simulated by using load control data," *Theoretical and Applied Fracture Mechanics* 27, 1-12. DOI:10.1016/S0167-8442(97)00002-5

Article submitted: July 28, 2015; Peer review completed: